Published in final edited form as:
J Exp Zool B Mol Dev Evol. 2012 March ; 318(2): 109–122. doi:10.1002/jezb.21449.

Unilateral and Bilateral Expression of a Quantitative Trait: Asymmetry and Symmetry in Coronal Craniosynostosis

YANN HEUZÉ[1], **NEUS MARTÍNEZ-ABADÍAS**[1], **JENNIFER M. STELLA**[1], **CRAIG W. SENDERS**[2], **SIMEON A. BOYADJIEV**[3], **LUN-JOU LO**[4], and **JOAN T. RICHTSMEIER**[1,*]

[1]Department of Anthropology, Pennsylvania State University, University Park, Pennsylvania

[2]Department of Otolaryngology, University of California Davis, Sacramento, California

[3]Section of Genetics, Department of Pediatrics, University of California Davis, Sacramento, California

[4]Department of Plastic and Reconstructive Surgery, Chang Gung Memorial Hospital, Chang Gung University, Taoyuan, Taiwan

Abstract

Bilateral symmetry in vertebrates is imperfect and mild asymmetries are found in normal growth and development. However, abnormal development is often characterized by strong asymmetries. Coronal craniosynostosis, defined here as consisting of premature suture closure and a characteristic skull shape, is a complex trait. The premature fusion of the coronal suture can occur unilaterally associated with skull asymmetry (anterior plagiocephaly) or bilaterally associated with a symmetric but brachycephalic skull. We investigated the relationship between coronal craniosynostosis and skull bilateral symmetry. Three-dimensional landmark coordinates were recorded on preoperative computed tomography images of children diagnosed with coronal nonsyndromic craniosynostosis ($N = 40$) and that of unaffected individuals ($N = 20$) and analyzed by geometric morphometrics. Our results showed that the fusion pattern of the coronal suture is similar across individuals and types of coronal craniosynostosis. Shape analysis showed that skulls of bilateral coronal craniosynostosis (BCS) and unaffected individuals display low degrees of asymmetry, whereas right and left unilateral coronal craniosynostosis (UCS) skulls are asymmetric and mirror images of one another. When premature fusion of the coronal suture (without taking into account cranial dysmorphology) is scored as a qualitative trait, the expected relationship between trait frequency and trait unilateral expression (i.e. negative correlation) is confirmed. Overall, we interpret our results as evidence that the same biological processes operate on the two sides in BCS skulls and on the affected side in UCS skulls, and that coronal craniosynostosis is a quantitative trait exhibiting a phenotypic continuum with BCS displaying more intense shape changes than UCS.

Bilateral symmetry, a key feature of vertebrate body plans, is never perfect and mild asymmetries are found in normal growth and development. Nondirectional deviations from perfect symmetry, measured as the differences between corresponding parts on the left and right sides of the body (i.e. fluctuating asymmetry) have been used to quantify the imprecision of developmental systems (i.e. developmental instability) in response to various stresses (Palmer and Strobeck, ’86; Møller and Swaddle, ’97; Klingenberg and McIntyre, ’98; Hallgrímsson, 2002; Klingenberg, 2003; Polak, 2003; Richtsmeier et al.,

*Correspondence to: Joan T. Richtsmeier, Department of Anthropology, Pennsylvania State University, 311 Carpenter Building, University Park, PA 16802, USA. jta10@psu.edu, jtr505@gmail.com.

2005). Deviation from perfect symmetry can also occur consistently on one side in terms of conformation or size of an organ (i.e. directional asymmetry). Visceral asymmetries or situs solitus (e.g. positioning of heart, liver, stomach) exhibit nonrandom laterality and represent the most fundamental exception to bilateral symmetry in vertebrates. In higher primates, the brain has also been shown to be asymmetric (directional asymmetry) in both its anatomy and functional organization (e.g. speech and language centers, visual and auditory preference, footedness and handedness).

Here, we investigate the relationship between coronal craniosynostosis, defined as consisting of premature suture closure and a characteristic dysmorphic skull shape, and skull bilateral symmetry. Sutures are joints between contiguous bones of the craniofacial skeleton. Normally, as individuals grow, the articulating bones expand in size, change in shape, and the sutures narrow, though bone does not form in the suture. When mature and patent, sutures include a thin layer of fibrous tissue that physically connects the margins of contiguous bones serving as a malleable interface for communicating tension and compression and for providing a free edge for the addition of osteogenic cells during skull growth. The maintenance of suture patency provides a functioning joint (Rafferty and Herring,'99; Herring et al., 2001; Sun et al., 2004; Popowics and Herring, 2007), as well as a dynamic area of growth potential to operate while continuing to protect the brain (Opperman, 2000). As individuals age, bone is deposited and the suture begins to "fuse," taking on the appearance of a hairline boundary between the bones. The formative coronal suture sits at the boundary between bones derived from two different embryonic tissues: the neural crest-derived mesenchyme that forms the frontal bone and the mesoderm-derived mesenchyme that forms the parietal bones of mammals (Jiang et al., 2002; Morriss-Kay and Wilkie, 2005; Merrill et al., 2006), but the implications of this finding for the development and epidemiology of coronal craniosynostosis remains incompletely understood.

Premature fusion of any of the cranial vault sutures is always associated with corresponding changes in skull shape, so that knowledge of the skull dysmorphology can usually predict the suture(s) that is (are) closed prematurely and knowledge of a closed suture can, in broad terms, predict overall skull shape. For example, metopic craniosynostosis involves premature fusion of the metopic suture and trigonocephaly, whereas sagittal craniosynostosis includes premature closure of the sagittal suture and scaphocephaly. Although bilateral coronal craniosynostosis (BCS) is not reported to affect bilateral symmetry of the skull, UCS is associated with marked asymmetry (Richtsmeier et al., 2005). The overt cranial shape associated with premature closure of the coronal suture varies depending upon whether premature closure of the coronal suture occurs unilaterally or bilaterally, the former being associated with anterior plagiocephaly, the latter being associated with an apparently symmetric but brachycephalic skull (Cohen and MacLean, 2000). In this article, the term coronal craniosynostosis is used to refer not only to the premature fusion of the coronal suture, but to the condition of the suture and the corresponding skull shape. It has long been thought that the premature closure of a suture restricts brain and skull growth in a direction perpendicular to that suture, whereas compensatory growth occurring at neighboring sutures contributes to the characteristic cranial shape. Recent works in mice carrying the two Fgfr2 mutations known to cause more than 98% of Apert syndrome cases (Aldridge et al., 2010; Martínez-Abadías et al., 2010) demonstrate that dysmorphology of skull bones can occur before suture closure occurs, suggesting that these craniosynostosis mutations have a more direct effect on skull growth and shape.

The incidence of craniosynostosis (potentially affecting any of the cranial vault sutures) is estimated to be in the range of 3–5 per 10,000 live births and occurs in all ethnic groups (Cohen and MacLean, 2000). Coronal craniosynostosis represents 20–30% of all cases and

affects twice as many females as males (Hunter et al., ’76; Lajeunie et al., ’98; Singer et al., ’99; Boyadjiev, 2007; Boulet et al., 2008). Unilateral coronal craniosynostosis (UCS) is estimated to occur 4–7 times as often as BCS, and right unilateral craniosynostosis (RUCS) is reported to occur twice as often as left unilateral coronal craniosynostosis (LUCS) (Boulet et al., 2008; Wilkie et al., 2010). Females are more often affected by left UCS than males, whereas the sex ratio is equivalent for right UCS (Seto et al., 2007).

Though environmental and genetic risk factors for craniosynostosis have been identified, no single risk factor has emerged as being necessary or sufficient to cause the condition. Mutations in at least seven genes and a large series of chromosomal abnormalities (affecting all autosomes) have been identified for patients presenting with syndromic craniosynostosis (Passos-Bueno et al., 2008). The coronal suture is prematurely fused in several craniosynostosis syndromes (e.g. Apert, Crouzon, Muenke, Pfeiffer, Saethre-Chotzen syndromes) which are caused by several different mutations, many of which are located on the genes coding for the fibroblast growth factor receptors (*FGFR*) 1, 2, and 3, and on *TWIST1* (Cohen and MacLean, 2000; Passos-Bueno et al., 2008). The FGF/FGFR signaling pathway mediates processes of proliferation, differentiation, migration, adhesion, and death of cells, including osteogenic cells (Ornitz and Marie, 2002; Hajihosseini, 2008). *TWIST1* is a gene coding for a transcription factor involved in cell lineage and differentiation. Several patients, initially diagnosed with isolated coronal craniosynostosis based on the absence of any anomaly other than the premature fusion of the coronal suture, have been found to carry single-gene mutations. These mutations are found on several genes, including: *FGFR2*, *FGFR3*, *TWIST1*, and *EFNA4* (Johnson et al., 2000; Merrill et al., 2006; Seto et al., 2007; Wilkie et al., 2010). Of these mutations, the FGFR3 P250R mutation causing Muenke syndrome is estimated to account for 5–8% of all craniosynostosis cases corresponding to a prevalence of 1 case per 30,000 living births (Wilkie et al., 2010).

The large number of mutations and various chromosomal anomalies spread throughout the genome that are associated with craniosynostosis (Passos-Bueno et al., 2008) suggest a polygenic basis for this condition. The identifiable genetic anomalies serve as susceptibility loci that interact with other genes whose contribution may be too small to reach statistical significance, but whose contribution in aggregate and with environmental influences combine to change development in such a way that an ultimate phenotypic outcome includes craniosynostosis (Johnson et al., 2000). These observations depict craniosynostosis as a complex trait and suggest that molecularly there may be many ways to the same end: premature suture closure associated with cranial dysmorphology. The first question we address is: when coronal craniosynostosis is analyzed as a quantitative trait, do cranial dysmorphologies associated with premature fusion of the coronal suture (whether unilateral or bilateral) display phenotypic discontinuity or form a phenotypic continuum?

Additionally, premature closure of a cranial suture, where the condition of the trait is defined as either “patent” or “closed,” can be thought as a qualitative trait. Data from quantitative and molecular genetics show that qualitative traits can be interpreted as occupying locations at the extremes of quantitative dimensions (Plomin et al., 2009). The genetic and environmental factors that operate in craniosynostosis are expected to be the same as those operating in the normal population and their aggregate distribution is expected to be normal (Falconer and Mackay, ’96). This distribution is perceived as an underlying multifactorial liability. The second question we address here is: regardless of the complexity of the molecular basis for coronal craniosynostosis, is premature closure of the coronal suture (whether unilateral or bilateral) the visible expression of the same biological and environmental factors where developmental processes are affected in similar ways?

We address these two questions through a comparative analysis of craniofacial morphology of LUCS, RUCS, BCS, and unaffected individuals (no craniofacial anomalies) using three-dimensional computed tomography (3D CT) images. The phenotypic variability of craniosynostosis is quantified by geometric morphometrics (GM) and by assessment of coronal suture fusion pattern. First, we test the hypothesis that in BCS both affected sides (i.e. the two sides with a prematurely fused suture) display a similar level of dysmorphology, implying that the developmental program is affected similarly on both sides and that bilateral symmetry is conserved (H1). Support for H1 would imply that the pattern and the timing of premature suture fusion are similar for both sides of the coronal suture and that the dysmorphology is bilaterally symmetric. If this was not the case, we would expect asymmetric features. Second, we test the hypothesis that LUCS and RUCS are products of the same biological processes that differ only in the laterality of their expression (H2). We test this hypothesis by determining whether RUCS and LUCS are mirror images of one other. If H2 is not supported, this would provide evidence for varying developmental programs being associated with UCS. Finally, we test the hypothesis that unilateral and bilateral craniosynostosis are the products of similar biological processes (H3). We test this hypothesis by determining if the coronal fusion patterns of the sides displaying premature fusion in BCS and of the side displaying premature fusion in UCS are similar. Additionally, using a data set in which premature fusion of the coronal suture is scored as a qualitative trait, we test the relationship between trait frequency and unilateral expression. Support for H3 would be provided if premature fusion of the coronal suture fits the model proposed by Hallgrímsson et al. (2005) advocating that qualitative traits are mainly expressed unilaterally, because they are rare and occur at the ends of phenotypic distributions for underlying liability parameters.

MATERIALS AND METHODS

Images

Computed tomography images of children diagnosed with coronal nonsyndromic craniosynostosis (coronal NSC, $N = 40$) and that of unaffected individuals ($N = 20$) were acquired from several US medical centers (Johns Hopkins Hospital; Children's Hospital of Boston; Children's Hospital of Los Angeles; St Joseph Hospital, Patterson; University of California Davis; University of Oklahoma Medical Center; Washington University), most of which participate in the International Craniosynostosis Consortium (https://genetics.ucdmc.ucdavis.edu/index.cfm). One coronal NSC case was recruited at the Chang Gung Memorial Hospital, Taiwan. Our control sample consists of images of children without craniosynostosis who underwent CT scanning for craniofacial conditions not associated with craniosynostosis (e.g. seizures, suspected brain anomalies). The CT images were deposited into our Image Analysis and Morphometrics Laboratory archive following IRB protocols of the Pennsylvania State University. Details of phenotype, sex, and age distributions are given in Table 1. Discrepancies between our clinic-based coronal craniosynostosis sample and the corresponding epidemiological data is mainly the consequence of two biases. The first is a case recruitment bias related to geographic location and clinical specialties available for craniosynostosis treatment at particular medical centers, and the other is a case selection bias related to the selection of only high-quality CT images for our analysis. At the time of CT exam, children with coronal craniosynostosis had not undergone any surgical procedure.

Individuals diagnosed with a known genetic syndrome were excluded and none of the individuals included in our study sample had extracranial anomalies. For 16 out of 40 individuals, a detailed evaluation was done by hot-spot mutation analysis of areas of the genome associated with known craniosynostosis syndromes (*FGFR1* exon IIIa, *FGFR2* exons IIIa and IIIc, *FGFR3* exon IIIa, and the entire coding sequence of the transcription

factor *TWIST1*). None of these 16 individuals carried any of the known mutations. Cases consequently consist of 16 individuals who did not express any of these known mutations and 24 individuals with a clinical diagnosis of coronal NSC for whom molecular data was not available.

Fusion of the Coronal Suture

All cases have premature fusion of the coronal suture but the exact condition of the coronal suture is not identical for all cases. We scored the condition of the suture visualized on each transverse CT slice passing through the coronal suture as patent or fused. To enable comparison of suture fusion patterns across CT studies of varying slice thickness and head sizes, the total number of CT slices in which the suture was visible (right and left sides examined separately) was divided equally by four to generate four coronal suture sections per side (A to D from the inferior to the superior part of the suture). Within each section, the mode of the slice suture scores (i.e. patent or fused) was used as the code for the entire section (Fig. 1). Once a code was obtained for each of the four sections of the right and left coronal suture, the four codes were assembled into a pattern of suture fusion. For example, a RUCS case with a right coronal suture totally fused and a left coronal suture totally patent will be coded as “FFFF” for the affected side (i.e. right) and “PPPP” for the left side. An individual presenting with BCS who displays left and right coronal sutures fused for the two first sections will be coded as “FFPP” for the two sides.

Landmark Data Collection and Shape Analysis

Images were reconstructed using a threshold that enabled visualization of bone. A set of 41 anatomical landmarks were defined and located on the 3D reconstruction of the CT images of each individual and the corresponding *x*, *y*, *z* coordinates were recorded (Fig. 2; details on the anatomical landmarks can be found at http://getahead.psu.edu/LandmarkNewVersion/Humanskull_Applet.html). The patent fontanelles visible on the 3D reconstructions of the CT images were manually closed using a segmentation tool to allow the placement of landmarks in these regions. In addition to the anatomical landmarks, 168 semilandmarks were defined on 11 predefined curves (92 curve semilandmarks; CL) and four surface patches (76 surface semilandmarks; SL) on each skull. In order to gain geometric correspondence, semilandmarks were slid along these curves and patches according to a sliding algorithm that minimizes the bending energy (Bookstein, ’97; Gunz et al., 2005). Avizo 6 (Visualization Sciences Group, SAS) was used to visualize the CT images, to segment and reconstruct the skulls, and to measure anatomical landmarks. The semilandmarks (CL and SL) were measured in Viewbox 4 (dHAL software, Athens, Greece).

The 40 coronal NSC cases and the 20 unaffected individuals defined on the basis of 209 landmarks (anatomical and semilandmarks combined) were superimposed by translating, rotating and scaling all forms with the aim of reducing the sum of the squared distances between homologous landmarks by means of generalized Procrustes analysis (Rohlf and Slice, ’90). The coordinates of the resulting centered, scaled, and rotated landmarks are called the Procrustes shape coordinates. A measure of overall size called centroid size (CS; the square root of the sum of the squared distances of the landmarks to the centroid) was estimated for each individual and used as a proxy for overall cranial size in subsequent analyses (Bookstein, ’91; Dryden and Mardia, ’98). The Procrustes average shape (PAS) is computed as the coordinate-wise average of the Procrustes shape coordinates.

The Procrustes shape coordinates were analyzed by principal components analyses (PCA) to reduce the dimensionality of the dataset and explore the placement of individuals within the shape space. One of the goals is to study the specific combination of morphological

variables that successfully separate individuals into groups of known membership by projecting them onto the shape space. The eigenvectors (or principal components (PCs)) contain the loadings for the linear combinations of the original variables and can be visualized as actual shape deformation. A simulation of a continuous shape deformation based on the available data can be obtained by warping the PAS to the negative (or positive) direction of the PC. This is done by adding a multiple of the eigenvector to the mean shape (PAS). Procrustes superimposition does not eliminate the allometric shape variation. Estimation of allometry is given by the multivariate regression of shape (all PCs; dependent variables) on size (CS; independent variable). The percentage of shape variation explained by size is given by the percentage predicted (percentage predicted = 1 − [sums of squares error/sums of squares total]). The null hypothesis of independence between shape and size is tested by permutation test (10,000 bootstraps) and a *P*-value is provided. In order to remove allometry from our analysis, we analyzed the residuals of the multivariate regression of shape on size in a new PCA.

Half-Skull Analysis

Because coronal craniosynostosis can occur unilaterally or bilaterally, it is possible to characterize the right and left sides of the skull according to the condition of the coronal suture. A side (i.e. half-skull) presenting premature fusion of the coronal suture would be called the “affected” side, whereas a side displaying a patent coronal suture would be called the “nonaffected” side. The term “nonaffected” side only refers to the absence of premature fusion of the coronal suture on that side and does not imply that the shape of the nonaffected side in UCS is normal.

Separation along the mid-sagittal plane produces two half-skulls: the left-sided half-skull including the anatomical landmarks and curve semilandmarks of the left side, and the right-sided half-skull including the right anatomical landmarks and right curve semilandmarks. Because for each individual the correspondence between a left surface semilandmark and its right counterpart is not guaranteed, surface semilandmarks were not used in the half-skull analysis. Because premature fusion of the coronal suture can break bilateral symmetry, we include data that reflect the relative position of “mid-line” structures in both half-skull composites, because they provide important information for each side of the skull. Consequently, unpaired anatomical landmarks lying on the mid-sagittal plane were included in both the left and right half-skulls.

Shape difference among groups of affected and nonaffected half-skulls was estimated using Procrustes distances. The Procrustes distance is a widely used measure of shape difference in GM and it is measured as the square root of the sum of squared distances between corresponding landmarks of two shape configurations after Procrustes superimposition (Dryden and Mardia, ’98). For each two-group comparison, the Procrustes distance between the two groups mean shapes was computed and a permutation test with 10,000 rounds was performed to test for statistical significance.

Symmetric and Asymmetric Components of Shape Variation

Several morphometric methods have been devised to study symmetry and asymmetry in objects with bilateral or matching symmetry. Here, we used the method devised by Klingenberg et al. (2002) for landmark configurations with object symmetry which partitions the total shape variation into components of symmetric and asymmetric variation by Procrustes superimposition of the original configurations and their mirror images. Before the superimposition, a reflected copy of each configuration is generated. Then, the paired landmarks of the reflected copies are relabeled so that each paired landmark obtains the label of its counterpart. To study the symmetric and asymmetric components of shape

variation, the Procrustes fit is accomplished using the original and mirrored configurations, superimposing all of them simultaneously. From this point, the process differs according to the shape variation component on which we focus. For the symmetric component of shape variation, the average of the original and mirrored configurations is done for each individual and results in a perfectly symmetric skull. The variation among individuals in these averages of original and reflected configurations constitutes the symmetric component of shape variation. The asymmetric component of shape variation is the difference between the original and mirrored configurations, and represents the landmark deviations of the original configuration from the symmetric consensus of the original and mirror image. Analyses of symmetric and asymmetric components of shape variation were done with MorphoJ (Klingenberg, 2011).

Relationship Between Trait Frequency and Unilateral Expression

Premature fusion of the coronal suture can be scored as a qualitative trait and interpreted as occupying the extremes of a continuous distribution of quantitative dimensions (Plomin et al., 2009). According to the threshold model for qualitative traits as developed in quantitative genetics, premature fusion of the coronal suture can be considered as having an underlying multifactorial (genetic and environmental) liability with a threshold which imposes a discontinuity on the visible expression of patency or fusion (Falconer and Mackay, ’96). Following this model, at an individual level, the genotypic variance for a threshold trait is expected to be similar for both sides (even though few genes have been shown to be expressed unilaterally; for a review, see Levin, 2005). However, the environmental variance can be similar for both sides or unique to each side, as it occurs in developmental instability (Hallgrímsson, 2002). Within-individual deviations can push both sides in the same direction (variance similar for both sides) or in opposite directions (variance unique to each side). Consequently, if the variance of the within-individual shifts that creates the asymmetry variance remains constant across the liability range, the number of individuals in which one side but not the other is pushed over the threshold for trait formation will be a larger proportion of the number of individuals expressing the trait when the trait frequency is low (Hallgrímsson et al., 2005). In other words, there is a strong negative correlation between the frequency of a threshold trait and unilateral expression.

Because our clinic-based sample is biased, we propose to test the relationship between the frequency of premature fusion of the coronal suture and the frequency of unilateral premature fusion of the coronal suture with acknowledged epidemiological frequencies. Let a, b, c, and d be the proportions of individuals presenting with coronal craniosynostosis (i.e. affected individuals), LUCS, RUCS, and BCS, respectively, so that $a = b+c+d$. A hypothetical sample of one million individuals will then contain 100 affected individuals (a), 28 LUCS (b), 57 RUCS (c), and 15 BCS (d). Based on these data and those provided by Hallgrímsson et al. (2005; Table 3), we compute the linear regression of trait frequency against the proportion of unilateral expression defined as $(b+c)/(b+c+d)$.

RESULTS

Suture Fusion Patterns

Figure 3 provides individual coronal suture fusion patterns for the two affected sides of BCS and the unique affected side of UCS skulls. The right and left sides of the unaffected individuals systematically displayed a patent coronal suture as did the nonaffected side of the UCS skulls (i.e. PPPP; not shown in Fig. 3). The affected sides of the BCS and UCS skulls displayed between one and four fused sections. In one BCS skull, the left side of the coronal suture displayed only a single fused section (i.e. PFPP). The majority of affected sides of individuals (38 affected sides corresponding to 29 individuals) were completely

fused (i.e. FFFF) at the time of 3D CT exam. Variation of suture fusion patterns for the remaining individuals is provided in Figure 3.

Analysis of Complete Skulls and All Landmarks and Semilandmarks

The PCA of the Procrustes shape coordinates using all landmarks and semilandmarks of the 40 coronal NSC cases and the 20 unaffected individuals reveals marked separation of phenotypes (i.e. LUCS, RUCS, BCS, and unaffected) on the plot of the first two PCs (Fig. 4A). However, no separation is observed according to sex. The first PC, accounting for 41.6% of the total variance, allowed separation of BCS skulls (negative values), UCS skulls (both RUCS and LUCS surround zero), and unaffected skulls (positive values) while PC2, accounting for 22.7% of the total variance, allowed separation of RUCS skulls (negative values) and LUCS skulls (positive values). Estimation of allometry is given by the multivariate regression between size (CS; independent variable) and shape (all PCs; dependent variables). In this analysis, size accounted for 14.0% of shape variation ($P<0.001$). Allometry was mainly expressed by PC1 for which size accounted for 28.6% of shape variation. The regression of skull size on age (Fig. 5) confirmed that the unaffected individuals and BCS cases differ in size; BCS skulls being smaller at equivalent age. However, LUCS and RUCS skull sizes were similar in size to skulls of unaffected individuals.

Figure 6 shows the mean shapes of the unaffected, LUCS, RUCS, and BCS skulls. Compared with unaffected individuals, the skulls of BCS individuals are reduced along the anteroposterior axis with a posterior projection of the frontal bone and the face associated with an anterior projection of the posterior aspect of the skull (cranial vault and middle and posterior cranial fossa) (Fig. 6A, C, F, and G). In the vertical dimension, an inferior projection of the cranial base is observed as well as a superior displacement of the mid and lower face (Fig. 6A, B, and C). Finally, BCS skulls display a wider biparietal dimension relative to the unaffected individuals (Fig. 6B, D–G). These major trends in skull shape differences between the unaffected individuals and the BCS cases correspond to shape changes associated with positive and negative values of PC1 (Fig. 4A) and reflect what is already known about BCS morphologies.

The second PC allowed separation of LUCS and RUCS skulls. Both LUCS and RUCS skulls display high degrees of asymmetry. The orbit of the synostosed side is shifted posterolaterally, whereas the other orbit is shifted anteromedially (Fig. 6B, E–G). The nasal aperture is shifted toward the affected side (Fig. 6B). The parietal (most lateral part) and squamous temporal of the nonaffected side are shifted posterolaterally, whereas the parietal (most lateral part) and squamous temporal of the affected side are shifted anteromedially (Fig. 6B, D, E, and G). The dome of the vault and middle cranial fossa are shifted toward the nonaffected side (Fig. 6B, E–G).

Our results confirm that the craniofacial dysmorphology associated with premature fusion of the coronal suture, whether occurring unilaterally or bilaterally, is not only restricted to the cranial vault but also occurs in the cranial base and the facial skeleton.

Half-Skull Analysis

Two groups can be created from half-skulls: (i) the nonaffected halves that correspond to the two halves of unaffected skulls and the nonaffected side of all UCS skulls, and (ii) the affected sides that correspond to the two sides of the BCS skulls and the affected side of all UCS skulls. The 120 half-skulls of the 60 children (40 coronal NSC cases plus 20 unaffected individuals) of the sample were superimposed using the anatomical landmarks and curve semilandmarks. The resulting Procrustes shape coordinates were used to run a PCA (not

shown). Because our sample consists of individuals ranging in age from 0 to 2 years old, a period of life where the skull experiences a dramatic increase in size, and because the sample displays age heterogeneity between phenotypes (Table 1), it was anticipated that size would be strongly associated with skull shape. As expected, size accounted for 16% of total shape variation ($P<0.001$) and for 32.6% of shape variation expressed by PC1.

Because size is confirmed to be one of the main factors influencing shape in this particular analysis, allometry has been removed by using the residuals of the multivariate regression of shape on size to run a new PCA (Fig. 7) (see Materials and Methods section). The first PC, accounting for 37.1% of the total variance, allowed separation of the nonaffected sides (negative values) from the affected sides (positive values). The main shape changes associated with PC1 are the orientation of the face relative to the neurocranium, the relative position of the frontal, the relative position of the cranial base, and the relative orientation of the occipital (Fig. 7). Those shape changes are similar to the ones associated with PC1 in the PCA of the Procrustes shape coordinates of the 60 entire skulls (Fig. 4A). The second PC, accounting for 23.1% of the total variance, allowed separation of nonaffected sides of the UCS cases from the affected sides. The main shape change associated with PC2 is the profile of the mid-sagittal plane. When the half-skulls are seen from a superior view, the affected sides display a bregma which forms the inflexion point of a convex profile, whereas the nonaffected sides display a bregma which forms the inflexion point of a concave profile (Fig. 7).

This resulted in separation of the data into four clusters: (i) the left and right half-skulls of the unaffected individuals in the upper left quadrant of the PCA, (ii) the left and right half-skulls of the BCS cases in the lower right quadrant, (iii) the nonaffected sides of the UCS skulls in the lower left quadrant, and (iv) the affected sides of the UCS skulls in the upper right quadrant. Procrustes distances among groups (i.e. left and right sides of unaffected, LUCS, RUCS, and BCS) are reported in Table 2. Only four group-pairs did not display significant differences: (i) the left and right sides of the unaffected individuals, (ii) the left and right sides of BCS skulls, (iii) the nonaffected sides of the UCS skulls, and (iv) the affected sides of the UCS skulls.

Finally, when the information concerning the age of the individuals is taken into account (not shown), each of the four clusters of the half-skull analysis display a trend with the youngest individuals on the left of the cluster and the oldest on the right.

Symmetric and Asymmetric Components of Shape Variation

After Procrustes superimposition of the original and mirrored configurations, the average of the original and mirrored configurations was done for each individual and resulted in a perfectly symmetric skull. The variation among individuals in these averages of original and reflected configurations constitutes the symmetric component of shape variation. The Procrustes shape coordinates of the average skulls were used to run a new PCA. The first PC accounting for 58.0% of the total variance allowed separation of the data into three groups: the unaffected skulls (negative values), the UCS skulls (around 0), and the BCS skulls (positive values) (Fig. 4B). The group formed by the UCS skulls did not display any separation of LUCS and RUCS skulls. Shape changes associated with PC1 were very similar to the ones associated with PC1 in the initial PCA (Fig. 4A).

Asymmetry is quantified through the landmark deviations of the original configuration from the symmetric consensus of the original and mirror image. The Procrustes shape coordinates of the differences between the original and mirrored skulls were used to run a new PCA. The first PC accounting for 78.3% of the total variance allowed separation of the data in three groups: the LUCS skulls (negative values), the unaffected and BCS skulls (around 0), and

the RUCS skulls (positive values) (Fig. 4C). Size has no significant influence on the asymmetric component of shape variation. The group formed by the less asymmetric skulls did not display any separation between unaffected individuals and BCS cases. Shape changes associated with PC1 were very similar to the ones associated with PC2 in the initial PCA (Fig. 4A).

Relationship Between Trait Frequency and Unilateral Expression

The linear regression of trait frequency against the proportion of unilateral expression defined as $(b+c)/(b+c+d)$ regrouping data from Hallgrímsson et al. (2005; Table 3) and data on premature fusion of the coronal suture is highly significant ($R = 0.79$, df = 27, $P<0.001$, regression slope: −0.62). The significance of directional asymmetry determined by a chi-square test as described by Green et al. (1979) indicates that premature fusion of the coronal suture displays significant directional asymmetry ($\chi^2 = 9.44$, $P<0.01$) with RUCS being more frequent than LUCS. The newly added point to the original linear regression published by Hallgrímsson et al. (2005) corresponding to the trait “premature fusion of the coronal suture” is not an outlier (residual within ±2 standard deviations), implying that premature fusion of the coronal suture fits the expected relationship between trait frequency and unilateral expression.

DISCUSSION

The fusion pattern of the coronal suture in coronal craniosynostosis as measured in this study suggests that the lower mid-section (section B) of the coronal suture is consistently the first to fuse, whereas the area closest to bregma (section D) is the last to fuse. Although there is some variation, the upper midsection (section C) is more commonly the second section to fuse prematurely (Fig. 3). Recently, we have shown that there was a consistent variation in the fusion pattern of the sagittal suture in sagittal NSC and that at least two distinct pathways toward complete sagittal suture fusion could be identified, each pathway being associated with specific cranial dysmorphologies (Heuzé et al., 2010). Here, we show that fusion pattern of the coronal suture in coronal craniosynostosis seems relatively less variable, this being consistent with a study based on a very small sample of individuals presenting with craniosynostosis (Albright and Byrd, ’81). Despite the complexity of the molecular basis for premature closure of the coronal suture, developmental processes seem to be affected in similar ways such that a consistent and predictable suture fusion pattern is produced.

Our results confirm previous reports of intense cranial base and facial shape changes in UCS and BCS in addition to the characteristic cranial vault dysmorphologies. However, a causal relationship between premature fusion of the coronal suture and facial or cranial base dysmorphology is difficult to establish and we cannot affirm that facial shape changes are the consequence of suture fusion or of neurocranial shape changes. For example, we have previously demonstrated with mouse models of Apert syndrome (*Fgfr2*$^{+/S252W}$ and *Fgfr2*$^{+/P253R}$, a craniosynostosis syndrome caused by mutation of FGFR2) that regardless of suture condition, the facial skeleton is primarily affected in mutant newborn mice (Martínez-Abadías et al., 2010).

Results from the analysis of the asymmetric component of shape variation (Fig. 4C) and from the half-skull analysis (Fig. 7; Table 2) show that skulls of BCS and unaffected individuals display comparable and relatively low degrees of asymmetry. These results support the hypothesis that in BCS the left and right sides of the skull display similar levels of dysmorphology thereby conserving bilateral symmetry (H1). The right and left coronal sutures of BCS skulls show similar closure patterns (Fig. 3) and the right and left sides of the skulls show similar levels of dysmorphology (Table 2), suggesting that either a single

process controls right and left suture closure and dysmorphogenesis or that BCS is the result of similar processes that affect the right and left sides separately but simultaneously. Results obtained from the analysis of the symmetric component of shape variation support the hypothesis that RUCS and LUCS skulls are mirror images of one another (H2) (Fig. 4B). The half-skull analysis also supports H2, because the affected sides of LUCS and RUCS skulls cluster together in the PCA plot as do the nonaffected side of the LUCS and RUCS skulls (Fig. 7; Table 2). We interpret this as evidence of a unique biological process generating UCS regardless of the laterality of the affected side.

Is the timing of the initiation of premature fusion of the coronal suture the same in BCS and in UCS? Because of the small sample size and differences in age distributions of the different subsamples (i.e. BCS, RUCS, LUCS; Table 1), no definitive answer can be given. The impression given by Figure 3 that the process starts earlier in UCS relative to BCS may be a consequence of the fact that UCS individuals are chronologically older than BCS individuals.

Though we cannot provide direct molecular and/or histological evidence from the cases presented here, correspondence between the coronal suture fusion patterns recorded for individuals with BCS and UCS suggests similarity in the biological processes generating the premature fusion of one side of the coronal suture in UCS and those that generate premature fusion on both sides of the coronal suture in BCS. Further support for the hypothesis that UCS and BCS result from similar biological processes is provided when premature fusion of the coronal suture is scored as a qualitative or nonmetric trait. Our results show that premature fusion of the coronal suture follows the expected relationship between trait frequency and unilateral expression. Although coronal craniosynostosis displays significant directional asymmetry which could imply a lesser dependence on trait frequency by reducing the role played by developmental instability, premature fusion of the coronal suture may be most frequently expressed unilaterally simply because it is rare (Hallgrímsson et al., 2005). If UCS and BCS were generated by different processes, we would expect an incompatibility between epidemiological data and the model. Our results provide support for the hypothesis that UCS and BCS are the products of similar biological processes (H3).

Craniosynostosis as a Quantitative Trait

Clinically, BCS is often considered a more severe phenotype than UCS (e.g. Doherty et al., 2007) and surgical outcome analysis reveals poorer results for individuals with BCS as compared to UCS. This latter observation has to be balanced by the higher proportion of syndromic cases presenting with BCS; syndromic cases who present with additional associated problems and abnormalities (Sloan et al., ’97; Arnaud et al., 2002; Seruya et al., 2011). The fact that patients presenting with BCS underwent preoperative CT imaging earlier than patients with UCS (Table 1) could be explained by considering isolated BCS as a more severe anomaly than isolated UCS. Females have been reported to present with coronal craniosynostosis twice as often as males (Hunter et al., ’76; Lajeunie et al., ’98; Singer et al., ’99; Boulet et al., 2008) and to be more severely affected by Muenke syndrome than males, presenting a higher proportion of bicoronal craniosynostosis relative to males (Gripp et al., ’98; Lajeunie et al., ’99; Cassileth et al., 2001; Doherty et al., 2007). Acknowledging that females might seek treatment at a craniofacial clinic more commonly than males because of stronger social and aesthetic pressures (Doherty et al., 2007), our bicoronal craniosynostosis clinic-based subsample displays a strong majority of females (12 for 3 males), and supports the hypothesis that females are not only more often, but also more severely affected by coronal craniosynostosis than males.

Severity as analyzed and discussed in this study relies only on morphological data. We quantified severity by estimating craniofacial shape variation as associated with the presence

or absence of premature closure of the coronal suture. The placement of the individuals on PC1 in the shape space when analyzed by PCA of the Procrustes shape coordinates using all landmarks and semilandmarks of the 60 individuals (Fig. 4A) supports the interpretation that BCS skulls display more intense shape changes than UCS skulls relative to control skulls. Indeed, relative to UCS skulls, BCS skulls are shorter in the anteroposterior axis, and display increased height and a wider biparietal dimension (Fig. 6). However, the separation of the individuals observed on PC1 represents only 41.6% of the total variance.

Further consideration of the half-skull analysis reveals a phenotypic continuum among the half-skulls where the most intense shape changes are consistently associated with the affected sides of BCS individuals (Fig. 7). Consequently, when PC1 scores are considered as phenotypic scores (Fig. 8), the distribution of cases along PC1 supports the hypothesis of a continuous distribution of phenotypes with unaffected skulls anchoring the negative end of PC1 and BCS skulls displaying more intense shape changes than UCS skulls. The fact that each of the four clusters of the half-skull analysis displays a trend with the youngest individuals on the left of the cluster and the oldest on the right implies that the intensity of the shape changes increases with age in all coronal craniosynostosis groups and that this is not because of a size effect on shape, because allometry has been removed in this particular analysis. These results coupled with those demonstrating that UCS and BCS are the consequences of similar biological processes support the view of coronal craniosynostosis as a quantitative trait. One interpretation of this statement is that it provides justification for grouping BCS and UCS for the purposes of genetic linkage and association studies and candidate gene analysis.

CONCLUSIONS

Although the detailed etiology of coronal craniosynostosis remains unknown, this study demonstrates that the dysmorphologies on the side displaying the premature fusion are similar regardless of the phenotype (i.e. LUCS, RUCS, or BCS) and mainly vary in term of intensity. We interpret our results as evidence that (i) the same biological processes operate to close the suture and change skull shape on the two sides in BCS and on the affected side in UCS, and that (ii) coronal craniosynostosis as a complex trait exhibits a phenotypic continuum with BCS displaying more intense shape changes than UCS.

Acknowledgments

We are grateful to all study participants and to the following persons who participated in the CT image collection and management: Jeffrey Marsh, St. Johns Mercy HealthCare system; Jayesh Panchal, University of Oklahoma; Alex Kane, Children's Medical Center Dallas; Benjamin Carson and Craig Vander Kolk, The Johns Hopkins University; Caroline Robson and Joan Stoler, Children's Hospital Boston; Pedro Sanchez-Lara, Children's Hospital of Los Angeles; James Boggan, University of California Davis. We thank the two anonymous reviewers whose comments helped to enhance the overall quality of the manuscript. S.A.B. is partially supported by Children's Miracle Network (CMN) endowed chair in Pediatric Genetics.

Grant Sponsor: Public Health Service; Grant numbers: R01 DE018500; 3R01 DE18500-02S1; R01 DE016886; CDC 5R01 DD000350.

LITERATURE CITED

Albright AL, Byrd RP. Suture pathology in craniosynostosis. J Neurosurg. 1981; 54:384–387. [PubMed: 7463140]

Aldridge K, Hill CA, Austin JR, Percival C, Martinez-Abadias N, Neuberger T, Wang Y, Jabs EW, Richtsmeier JT. Brain phenotypes in two FGFR2 mouse models for Apert syndrome. Dev Dyn. 2010; 239:987–997. [PubMed: 20077479]

Arnaud E, Meneses P, Lajeunie E, Thorne JA, Marchac D, Renier D. Postoperative mental and morphological outcome for nonsyndromic brachycephaly. Plast Reconstr Surg. 2002; 110:6–12. [PubMed: 12087222]

Bookstein, FL. Morphometric tools for landmark data: geometry and biology. Cambridge: Cambridge University Press; 1991.

Bookstein FL. Landmark methods for forms without landmarks: morphometrics of group differences in outline shape. Med Image Anal. 1997; 1:225–243. [PubMed: 9873908]

Boulet SL, Rasmussen SA, Honein MA. A population-based study of craniosynostosis in metropolitan Atlanta, 1989–2003. Am J Med Genet A. 2008; 146A:984–991. [PubMed: 18344207]

Boyadjiev SA. Genetic analysis of non-syndromic craniosynostosis. Orthod Craniofac Res. 2007; 10:129–137. [PubMed: 17651129]

Cassileth LB, Bartlett SP, Glat PM, Gripp KW, Muenke M, Zackai EH, Whitaker LA. Clinical characteristics of patients with unicoronal synostosis and mutations of fibroblast growth factor receptor 3: a preliminary report. Plast Reconstr Surg. 2001; 108:1849–1854. [PubMed: 11743367]

Cohen, MM.; MacLean, RE. Craniosynostosis: diagnosis, evaluation, and management. 2. New York: Oxford University Press; 2000.

Doherty ES, Lacbawan F, Hadley DW, Brewer C, Zalewski C, Kim HJ, Solomon B, Rosenbaum K, Domingo DL, Hart TC, Brooks BP, Immken L, Lowry RB, Kimonis V, Shanske AL, Jehee FS, Bueno MR, Knightly C, McDonald-McGinn DM, Zackai EH, Muenke M. Muenke syndrome (FGFR3-related craniosynostosis): expansion of the phenotype and review of the literature. Am J Med Genet A. 2007; 143A:3204–3215. [PubMed: 18000976]

Dryden, IL.; Mardia, KV. Statistical shape analysis. Chichester: John Wiley & Sons; 1998.

Falconer, DS.; Mackay, TFC. Introduction to quantitative genetics. London: Longman; 1996.

Green RF, Suchey JM, Gokhale DV. The statistical treatment of correlated bilateral traits in the analysis of cranial material. Am J Phys Anthropol. 1979; 50:629–634. [PubMed: 464034]

Gripp KW, McDonald-McGinn DM, Gaudenz K, Whitaker LA, Bartlett SP, Glat PM, Cassileth LB, Mayro R, Zackai EH, Muenke M. Identification of a genetic cause for isolated unilateral coronal synostosis: a unique mutation in the fibroblast growth factor receptor 3. J Pediatr. 1998; 132:714–716. [PubMed: 9580776]

Gunz, P.; Mitteroecker, P.; Bookstein, FL. Semilandmarks in three dimensions. In: Slice, DE., editor. Modern morphometrics in physical anthropology. New York: Kluwer Academic/Plenum Publishers; 2005. p. 73-98.

Hajihosseini MK. Fibroblast growth factor signaling in cranial suture development and pathogenesis. Front Oral Biol. 2008; 12:160–177. [PubMed: 18391500]

Hallgrímsson, B. Phenotypic stability. In: Pagel, MD., editor. Oxford encyclopedia of evolutionary biology. New York: Oxford University Press; 2002. p. 886-891.

Hallgrímsson B, Donnabháin BO, Blom DE, Lozada MC, Willmore KT. Why are rare traits unilaterally expressed? Trait frequency and unilateral expression for cranial nonmetric traits in humans. Am J Phys Anthropol. 2005; 128:14–25. [PubMed: 15778959]

Herring SW, Rafferty KL, Liu ZJ, Marshall CD. Jaw muscles and the skull in mammals: the biomechanics of mastication. Comp Biochem Physiol, Part A Mol Integr Physiol. 2001; 131:207–219.

Heuzé Y, Boyadjiev SA, Marsh JL, Kane AA, Cherkez E, Boggan JE, Richtsmeier JT. New insights into the relationship between suture closure and craniofacial dysmorphology in sagittal nonsyndromic craniosynostosis. J Anat. 2010; 217:85–96. [PubMed: 20572900]

Hunter AG, Rudd NL, Hoffmann HJ. Trigonocephaly and associated minor anomalies in mother and son. J Med Genet. 1976; 13:77–79. [PubMed: 1271432]

Jiang X, Iseki S, Maxson RE, Sucov HM, Morriss-Kay GM. Tissue origins and interactions in the mammalian skull vault. Dev Biol. 2002; 241:106–116. [PubMed: 11784098]

Johnson D, Wall SA, Mann S, Wilkie AO. A novel mutation, Ala315Ser, in FGFR2: a gene-environment interaction leading to craniosynostosis? Eur J Hum Genet. 2000; 8:571–577. [PubMed: 10951518]

Klingenberg, CP. A developmental perspective on developmental instability: theory, models and mechanisms. In: Polak, M., editor. Developmental instability: causes and consequences. New York: Oxford University Press; 2003. p. 14-31.

Klingenberg CP. MorphoJ: an integrated software package for geometric morphometrics. Mol Ecol Resour. 2011; 11:353–357. [PubMed: 21429143]

Klingenberg CP, McIntyre GS. Geometric morphometrics of developmental instability: analyzing patterns of fluctuating asymmetry with Procrustes methods. Evolution. 1998; 52:1363–1375.

Klingenberg CP, Barluenga M, Meyer A. Shape analysis of symmetric structures: quantifying variation among individuals and asymmetry. Evolution. 2002; 56:1909–1920. [PubMed: 12449478]

Lajeunie E, Le Merrer M, Marchac D, Renier D. Syndromal and nonsyndromal primary trigonocephaly: analysis of a series of 237 patients. Am J Med Genet. 1998; 75:211–215. [PubMed: 9450889]

Lajeunie E, El Ghouzzi V, Le Merrer M, Munnich A, Bonaventure J, Renier D. Sex related expressivity of the phenotype in coronal craniosynostosis caused by the recurrent P250R FGFR3 mutation. J Med Genet. 1999; 36:9–13. [PubMed: 9950359]

Levin M. Left-right asymmetries in embryonic development: a comprehensive review. Mech Dev. 2005; 122:3–25. [PubMed: 15582774]

Martínez-Abadías N, Percival C, Aldridge K, Hill CA, Ryan T, Sirivunnabood S, Wang Y, Jabs EW, Richtsmeier JT. Beyond the closed suture in apert syndrome mouse models: evidence of primary effects of FGFR2 signaling on facial shape at birth. Dev Dyn. 2010; 239:3058–3071. [PubMed: 20842696]

Merrill AE, Bochukova EG, Brugger SM, Ishii M, Pilz DT, Wall SA, Lyons KM, Wilkie AOM, Maxson RE. Cell mixing at a neural crest-mesoderm boundary and deficient ephrin-Eph signaling in the pathogenesis of craniosynostosis. Hum Mol Genet. 2006; 15:1319–1328. [PubMed: 16540516]

Møller, AP.; Swaddle, JP. Asymmetry, developmental stability, and evolution. Oxford: Oxford University Press; 1997.

Morriss-Kay GM, Wilkie AOM. Growth of the normal skull vault and its alteration in craniosynostosis: insights from human genetics and experimental studies. J Anat. 2005; 207:637–653. [PubMed: 16313397]

Opperman LA. Cranial sutures as intramembranous bone growth sites. Dev Dyn. 2000; 219:472–485. [PubMed: 11084647]

Ornitz DM, Marie PJ. FGF signaling pathways in endochondral and intramembranous bone development and human genetic disease. Genes Dev. 2002; 16:1446–1465. [PubMed: 12080084]

Palmer AR, Strobeck C. Fluctuating asymmetry: measurement, analysis, patterns. Annu Rev Ecol Syst. 1986; 17:391–421.

Passos-Bueno MR, Serti Eacute AEAL, Jehee FS, Fanganiello R, Yeh E. Genetics of craniosynostosis: genes, syndromes, mutations and genotype-phenotype correlations. Front Oral Biol. 2008; 12:107–143. [PubMed: 18391498]

Plomin R, Haworth CMA, Davis OSP. Common disorders are quantitative traits. Nat Rev Genet. 2009; 10:872–878. [PubMed: 19859063]

Polak, M. Developmental instability: causes and consequences. New York: Oxford University Press; 2003.

Popowics TE, Herring SW. Load transmission in the nasofrontal suture of the pig, Sus scrofa. J Biomech. 2007; 40:837–844. [PubMed: 16690062]

Rafferty KL, Herring SW. Craniofacial sutures: morphology, growth, and in vivo masticatory strains. J Morphol. 1999; 242:167–179. [PubMed: 10521876]

Richtsmeier, JT.; Cole, TM.; Lele, SR. An invariant approach to the study of fluctuating asymmetry: developmental instability in a mouse model for down syndrome. In: Slice, DE., editor. Modern morphometrics in physical anthropology. New York: Kluwer Academic/Plenum Publishers; 2005. p. 187-212.

Rohlf F, Slice D. Extensions of the Procrustes method for the optimal superimposition of landmarks. Syst Zool. 1990; 39:40–59.

Seruya M, Oh AK, Boyajian MJ, Posnick JC, Myseros JS, Yaun AL, Keating RF. Long-term outcomes of primary craniofacial reconstruction for craniosynostosis: a 12-year experience. Plast Reconstr Surg. 2011; 127:2397–2406. [PubMed: 21311385]

Seto ML, Hing AV, Chang J, Hu M, Kapp-Simon KA, Patel PK, Burton BK, Kane AA, Smyth MD, Hopper R, Ellenbogen RG, Stevenson K, Speltz ML, Cunningham ML. Isolated sagittal and coronal craniosynostosis associated with TWIST box mutations. Am J Med Genet A. 2007; 143:678–686. [PubMed: 17343269]

Singer S, Bower C, Southall P, Goldblatt J. Craniosynostosis in Western Australia, 1980–1994: a population-based study. Am J Med Genet. 1999; 83:382–387. [PubMed: 10232748]

Sloan GM, Wells KC, Raffel C, McComb JG. Surgical treatment of craniosynostosis: outcome analysis of 250 consecutive patients. Pediatrics. 1997; 100:E2. [PubMed: 9200376]

Sun Z, Lee E, Herring SW. Cranial sutures and bones: growth and fusion in relation to masticatory strain. Anat Rec A Discov Mol Cell Evol Biol. 2004; 276:150–161. [PubMed: 14752854]

Wilkie AOM, Byren JC, Hurst JA, Jayamohan J, Johnson D, Knight SJL, Lester T, Richards PG, Twigg SRF, Wall SA. Prevalence and complications of single-gene and chromosomal disorders in craniosynostosis. Pediatrics. 2010; 126:e391–400. [PubMed: 20643727]

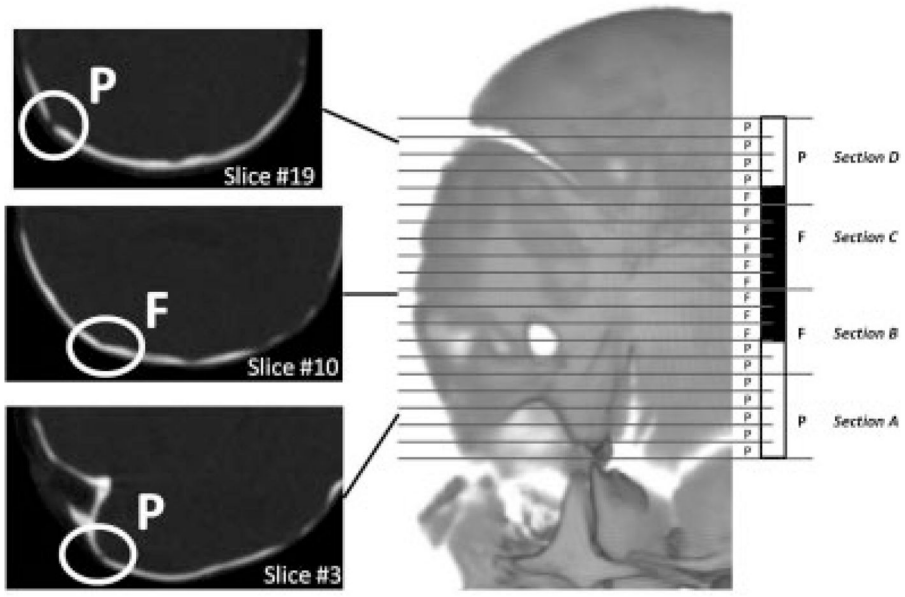

Figure 1.
Diagram illustrating the method used to code coronal suture fusion. In this example, the left side of the coronal suture corresponds to 20 CT slices. The coronal suture visualized on each CT slice is scored as patent (P, white) or fused (F, black) according to the coronal suture condition. The 20 slices are then divided in four equal sections of five slices each and the sections are coded as patent or fused according to the mode of the distribution of the scores of their slices.

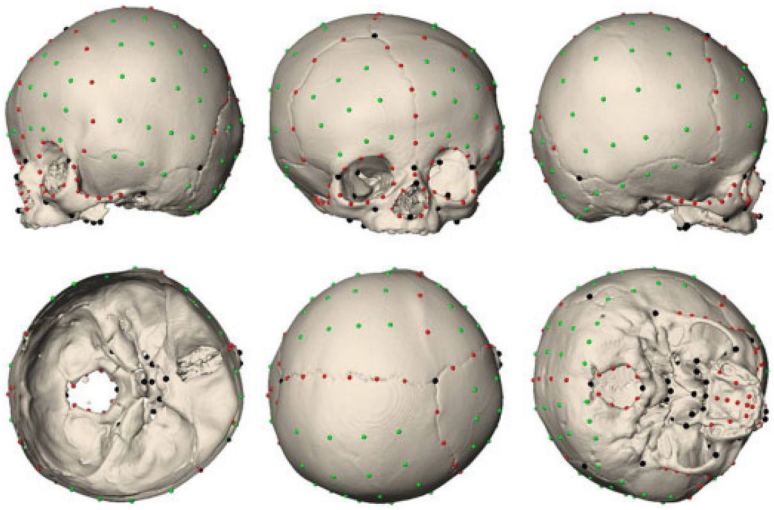

Figure 2.
Illustration of the 209 points measured on 3D reconstruction of the CT images of each individual in our sample (LUCS skull shown here). Anatomical landmarks are shown in black, curve semilandmarks are shown in red, and surface semilandmarks are shown in green.

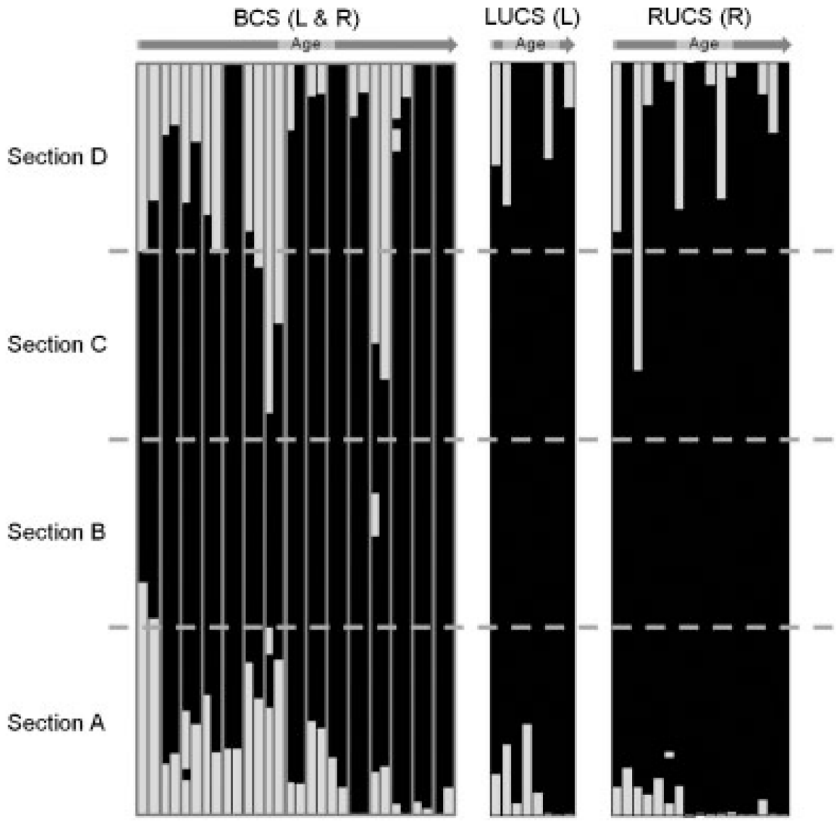

Figure 3.
Coronal suture fusion patterns by phenotype and age. Each bar represents one side of the coronal suture. For the BCS cases, each doublet of bars represents the left, then right suture (the two bars corresponding to one individual being framed in grey). Only the affected side is shown for the UCS cases. The white and black sections represent the slices where the coronal suture was patent and fused, respectively. Though coronal suture can be represented by 20 or 100 slices depending on the CT slice thickness, all bars have been resized to a common height.

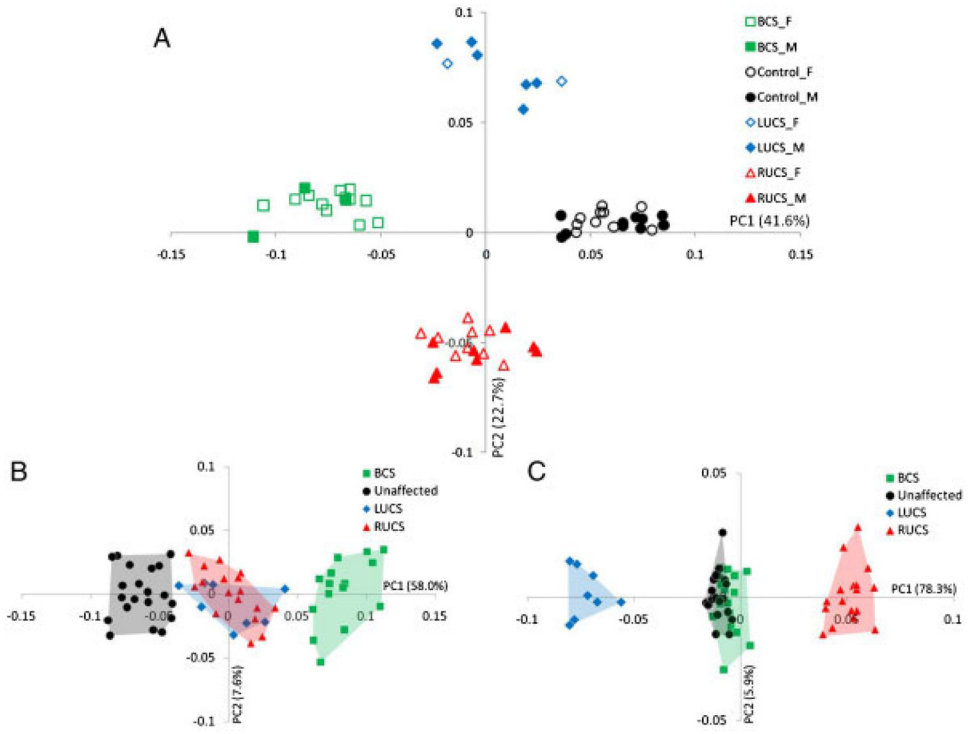

Figure 4.

(A) Placement of the individuals on PC1 and PC2 in the shape space (principal components analysis of the Procrustes shape coordinates using all landmarks and semilandmarks of the 60 individuals). Boys are denoted by filled symbols while empty symbols denote girls. Unaffected, LUCS, RUCS, and BCS skulls are represented by circles, diamonds, triangles, and squares, respectively. (B) Placement of the individuals on PC1 and PC2 when the symmetric component of shape variation is studied. (C) Placement of the individuals on PC1 and PC2 when the asymmetric component of shape variation is studied.

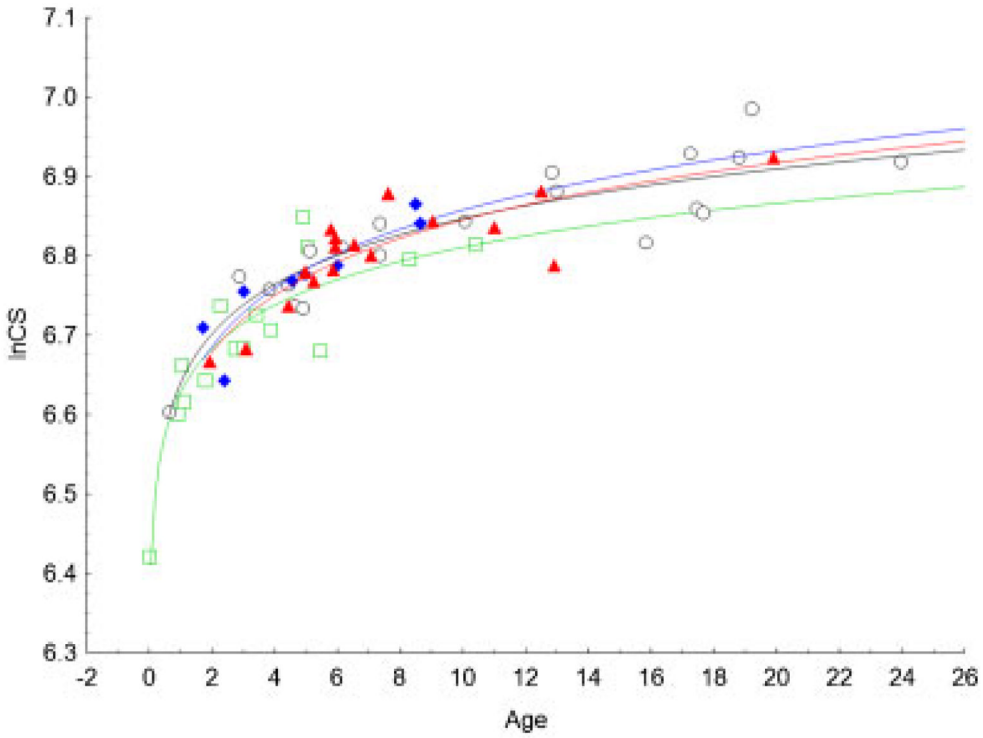

Figure 5.
Regression of skull size (lnCS) on age (months). Unaffected: open black circles; BCS: green open squares; LUCS: full blue diamonds; RUCS: full red triangles. Logarithmic fitting is represented for unaffected (black curve), BCS (green curve), LUCS (blue curve), and RUCS (red curve).

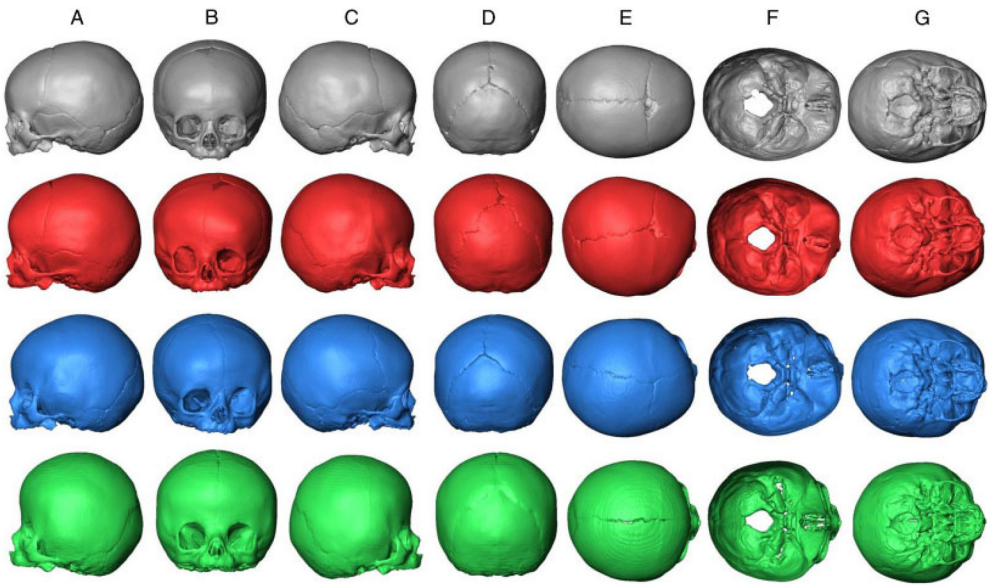

Figure 6.
Procrustes average shape (PAS) of unaffected skulls (first row, black), PAS of RUCS skulls (second row, red), PAS of LUCS skulls (third row, blue), and PAS of BCS skulls (fourth row, green). A: lateral (left) view; B: anterior view; C: lateral (right) view; D: posterior view; E: superior view; F: endocranial base view; G: ectocranial base (inferior) view.

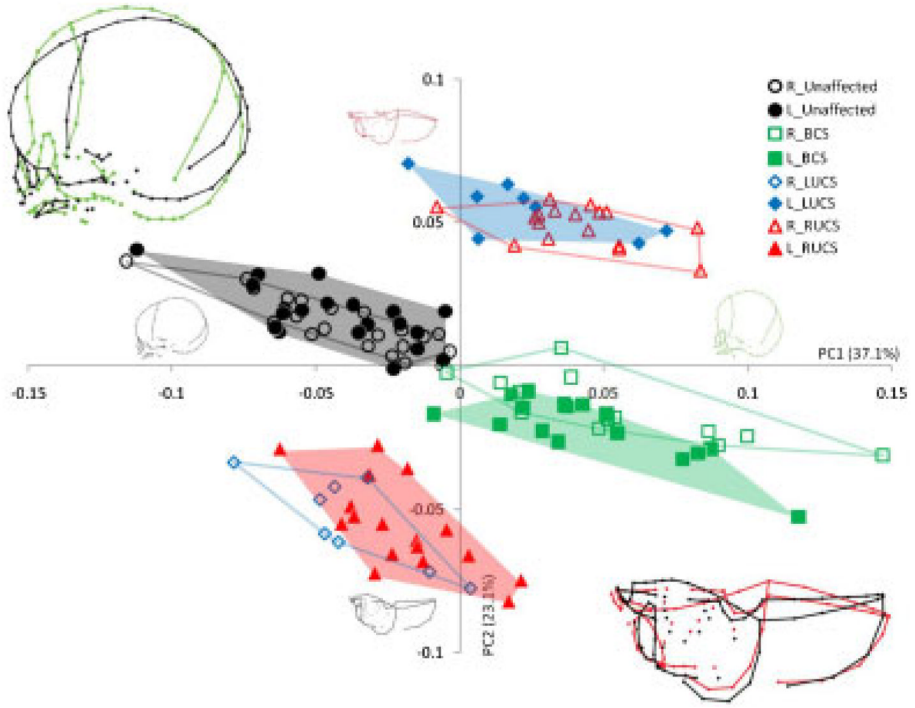

Figure 7.

Placement of the half-skulls on PC1 and PC2 in the shape space after adjusting for allometry. Different convex hulls are drawn for the left and right bicoronal, left unicoronal, right unicoronal, and unaffected half-skull. Wireframe graphs representing the shape changes associated with positive and negative values of PC1 in lateral view and the shape changes associated with positive and negative values of PC2 in superior view are represented for each PC and superimposed in the top left corner and the bottom right corner, respectively.

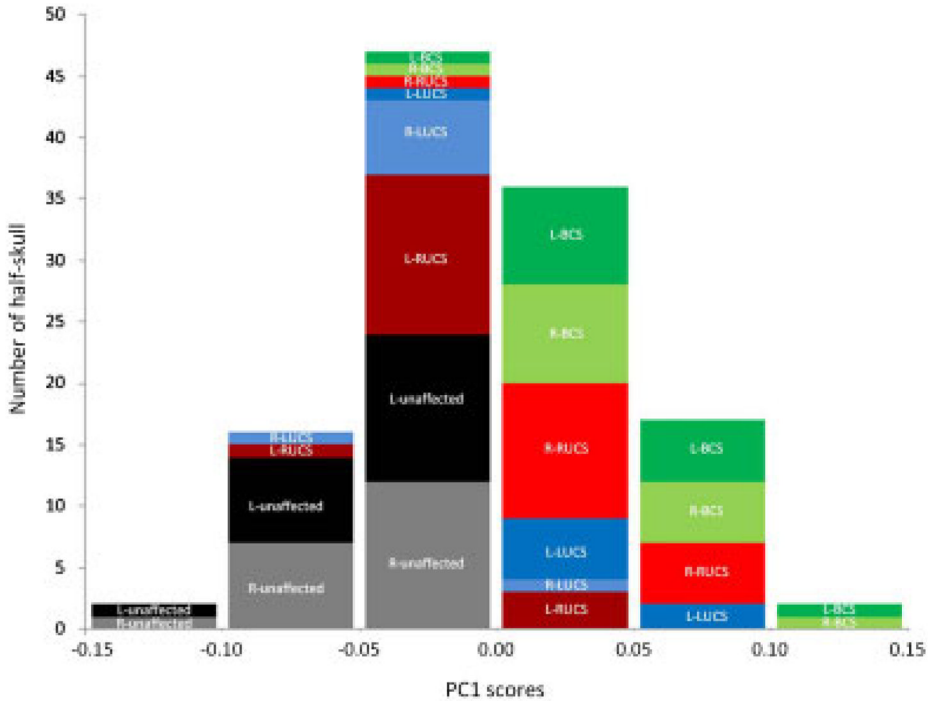

Figure 8.
Distribution of half-skull phenotypes according to PC1 scores obtained with the PCA of the half-skulls once allometry has been removed as in Figure 7.

Table 1

Age and sex distribution by phenotype

	Females		Males	
Phenotype	***n***	**Mean age in months (SD)**	***n***	**Mean age in months (SD)**
Unaffected	10	7.4 (5.9)	10	14.0 (6.2)
LUCS	2	5.2 (4.9)	6	4.9 (2.2)
RUCS	9	5.5 (2.5)	8	10.0 (4.9)
BCS	12	3.2 (2.3)	3	5.5 (4.7)

Table 2

Procrustes distances among groups in the half-skull analysis

	L-BCS	L-Control	L-LUCS	L-RUCS	R-BCS	R-Control	R-LUCS
L-Control	0.0978 (<.0001)						
L-LUCS	0.0829 (<.0001)	0.0803 (<.0001)					
L-RUCS	0.0755 (<.0001)	0.0787 (<.0001)	0.1214 (<.0001)				
R-BCS	**0.0207 (0.7686)**	0.1016 (<.0001)	0.0792 (<.0001)	0.0848 (<.0001)			
R-Control	0.0966 (<.0001)	**0.0127 (0.8737)**	0.0813 (<.0001)	0.0765 (<.0001)	0.0989 (<.0001)		
R-LUCS	0.0928 (<.0001)	0.0768 (<.0001)	0.1269 (0.0001)	**0.0303 (0.0759)**	0.0995 (<.0001)	0.073 (<.0001)	
R-RUCS	0.0743 (<.0001)	0.0915 (<.0001)	**0.0283 (0.1249)**	0.1221 (<.0001)	0.0672 (<.0001)	0.0909 (<.0001)	0.1308 (<.0001)

P-values from 10,000 permutation tests. Bold distances and *P*-values indicate nonsignificant differences.